

DOI: 10.1002/cctc.201200923

Painting Anatase (TiO₂) Nanocrystals on Long Nanofibers to Prepare Photocatalysts with Large Active Surface for Dye Degradation and Organic Synthesis

Zhanfeng Zheng, Jian Zhao, Hongwei Liu, Jiangwen Liu, Arixin Bo, and Huaiyong Zhu^{*[a]}

Anatase TiO₂ nanocrystals were painted on H-titanate nanofibers by using an aqueous solution of titanyl sulfate. The anatase nanocrystals were bonded solidly onto the titanate fibers through formation of coherent interfaces at which the oxygen atoms were shared by the nanocrystals and the fiber. This approach allowed us to create large anatase surfaces on the nanofibers, which are active in photocatalytic reactions. This method was also applied successfully to coat anatase nanocrystals on surfaces of fly ash and layered clay. The painted nanofibers exhibited a much higher catalytic activity for the photocatalytic degradation of sulforhodamine B and the selective oxidation of benzylamine to the corresponding imine (with a product selectivity > 99%) under UV irradiation than both the parent H-titanate nanofibers and a commercial TiO₂


powder, P25. We found that gold nanoparticles supported on H-titanate nanofibers showed no catalytic activity for the reduction of nitrobenzene to azoxybenzene, whereas the gold nanoparticles supported on the painted nanofibers and P25 could efficiently reduce nitrobenzene to azoxybenzene as the sole product under visible light irradiation. These results were different from those from the reduction on the gold nanoparticles photocatalyst on ZrO₂, in which the azoxybenzene was the intermediate and converted to azobenzene quickly. Evidently, the support materials significantly affect the product selectivity of the nitrobenzene reduction. Finally, the new photocatalysts could be easily dispersed into and separated from a liquid because of their fibril morphology, which is an important advantage for practical applications.

Introduction

TiO₂ photocatalysts, especially the solids of anatase phase that are the most studied photocatalyst materials, have drawn great attention because of their ability to degrade organic pollutants in wastewater and air completely and because of their chemical and thermal stability.^[1–3] Generally, a large active surface of the photocatalyst is very important for photocatalytic reactions because the photocatalytic reactions take place on the surface.^[4–8] Photocatalysts made of small particles have large active surfaces but they suffer from particle aggregation and a poor photocatalyst recovery for reuse.^[9,10] A feasible approach is to immobilize the small active particles on a substrate. By such an approach, one can effectively control particle aggregation and achieve large active surfaces for catalytic reactions. The large dimension of the substrate plays an important role in the dispersion and stabilization of the discrete nanoparticles. Generally, the recovery of catalysts obtained by such an approach for reuse is much easier than that of small particles. Thus, methods to immobilize small active particles are of significant importance and have been widely studied.^[11–14]

On the other hand, photocatalysis is, in principle, desirable for the synthesis of organic chemicals as the process generally proceeds at ambient temperature; and solid photocatalysts may be readily recovered after use. Nonetheless, if used for organic synthesis, TiO₂ photocatalysts exhibit poor product selectivity, especially in aqueous solution, owing to the generation of OH[•] radicals and the autoxidation of the photogenerated radicals.^[4,15] These radicals have strong oxidation power and can oxidize organic compounds completely. Recently, high selectivity has been achieved in an organic solvent as the unselective process driven by the radicals was inhibited.^[15–19] If photocatalysts with a large active surface can be attained, they may be efficient catalysts for the synthesis of organic chemicals through selective oxidation. Moreover, the immobilized TiO₂ may also be a superior support of Au nanoparticle (NP) photocatalysts. The metal oxide support with a large surface area allows Au NPs to disperse into discrete NPs, which are beneficial for their catalytic performance. Au NPs can strongly absorb visible light because of the surface plasmon resonance (SPR) effect, and the light absorption could induce the reaction of the molecules on the NPs such as the selective reduction of nitrobenzene under visible light irradiation.^[20–22] The photocatalysis process follows a different pathway from that of a process under elevated temperature and pressure using the Au NP catalyst on TiO₂.^[23] The Au NP photocatalysts on transition metal oxides usually exhibit much better activity than those on other oxide supports.^[20–21] A rational supposition is that the

[a] Dr. Z. Zheng, J. Zhao, Dr. H. Liu, Dr. J. Liu, A. Bo, Prof. H. Zhu
School of Chemistry, Physics and Mechanical Engineering
Queensland University of Technology
Brisbane, QLD 4001 (Australia)
Fax: (+61) 7-3138-1804
E-mail: hy.zhu@qut.edu.au

 Supporting information for this article is available on the WWW under <http://dx.doi.org/10.1002/cctc.201200923>.

support materials of the Au NP photocatalysts have important influence on the catalyst performance.

In the present study we painted TiO₂ nanocrystals (NCs) on the surface of H-titanate nanofibers (NFs) using titanyl sulfate (TiOSO₄) as the Ti source, generating a large active anatase surface on the inactive substrate of H-titanate. The large anatase surfaces were adequately exposed to reactant molecules, and the painted nanofibers could be easily dispersed into liquids and be recovered from a liquid by filtration or sedimentation. The fibril photocatalysts exhibited high activities in two reactions: 1) the degradation of sulforhodamine B (SRB) under UV light and 2) the selective oxidation of benzylamine to the corresponding imine under UV light. Au NPs as photocatalysts on the painted NFs exhibited high activity for the photocatalytic reduction of nitrobenzene to azoxybenzene under visible light. The last two reactions are important in industry for producing fine chemicals and pharmaceuticals and have been widely studied.^[15,21,24–26]

Results and Discussion

Surface, crystal structure, morphology, and UV/Vis absorption properties

N₂ adsorption–desorption isotherms of H-titanate NFs and anatase NCs painted NFs (TA-S12) are shown in Figure 1. The anatase NC painting resulted in a dramatic increase in the specific surface area, from 23 m²g⁻¹ for H-titanate to 166 m²g⁻¹ for TA-S12. TA-S12 displayed type-IV adsorption isotherms typical of mesoporous materials,^[27] with average pore sizes in the 3–6 nm range. These mesopores should be the intercrystal voids within the NCs. In contrast, a type-II adsorption isotherm without hysteresis loop is observed for the pristine H-titanate NFs, indicating that the sample is a nonporous solid.^[27]

The XRD patterns of H-titanate NFs and TA-S12 are shown in Figure 2a. The H-titanate NFs were indexed as H₂Ti₃O₇,^[28,29] whereas the diffraction peak of anatase (011) is clearly observed in TA-S12. There are diffraction peaks from both anatase and titanate in TA-S12, indicating that the sample contained the two phases. The TEM images in Figure 2 illustrate an interesting morphological evolution of the TA-S12. The substrate H-titanate NFs had a relatively smooth surface (Figure 2b). The painting resulted in a very rough surface; anatase NCs with sizes of approximately 6 nm can be clearly seen on the TA-S12 NFs (Figure 2c). This result also confirms that the mesopores of the sample are the intercrystal voids among the NCs. In an HRTEM image of an anatase particle (Figure 2d), the spacing between the parallel fringes was 0.35 nm, consistent with the lattice spacing of the anatase (011) plane. In our previous work, large anatase crystals (sized at ≈40 nm) that covered H-titanate NFs were obtained from the H-titanate NFs in a diluted acid solution (0.05 M HNO₃) at moderate hydrothermal conditions (110 °C).^[10] In the present study, the much smaller anatase NCs on H-titanate NFs were obtained at a much lower temperature and weaker acid conditions (80 °C, pH ≈2.6). No anatase crystals formed when treating H-titanate NFs at the same acidity and temperature in the absence of TiOSO₄.

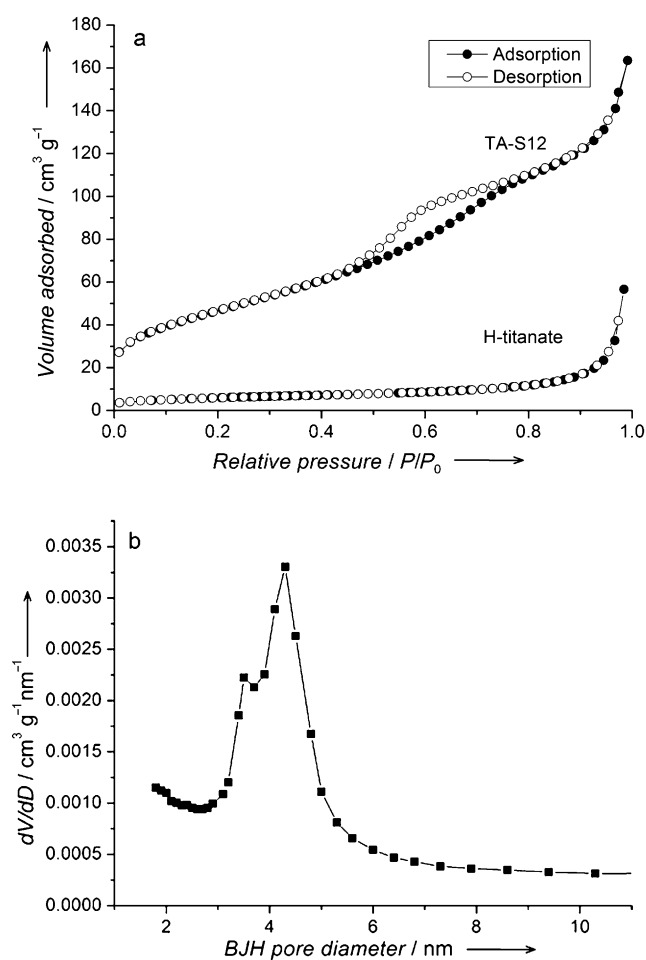


Figure 1. a) N₂ adsorption–desorption isotherms of H-titanate and TA-S12. b) The Barrett–Joyner–Halenda (BJH) pore size distribution of TA-S12.

If these nanofibers were used as supports for loading gold, the Au NPs uniformly deposited on the two types of nanofibers, as shown in Figure 2e and f. The Au particle size distributions are shown in Figure 2g. On both supports, the sizes of Au NPs are mainly (>90%) distributed from 3 to 8 nm. For comparison, Au NPs were also loaded on the reference P25 and the size of Au NPs on it was also mainly distributed in this range (see the Supporting Information, Figure S1). The diffuse reflectance UV/Vis spectra (Figure 3) of supported Au NPs all exhibited a broad surface plasmon resonance peak at approximately 540 nm, which also confirmed the similar Au particle size.^[21,30–32]

Anatase NCs growth mechanism study

In Figure 4, the XRD patterns and Raman spectra of the solids obtained from titanyl sulfate solution after treatment at 80 °C for time periods from 1 h to 48 h in the absence of the H-titanate NFs are shown. The patterns reveal the structural evolution of the precursor of the anatase NCs during the hydrothermal treatment at 80 °C. As seen from the Raman spectra, the product obtained from 1 h treatment exhibited typical vibra-

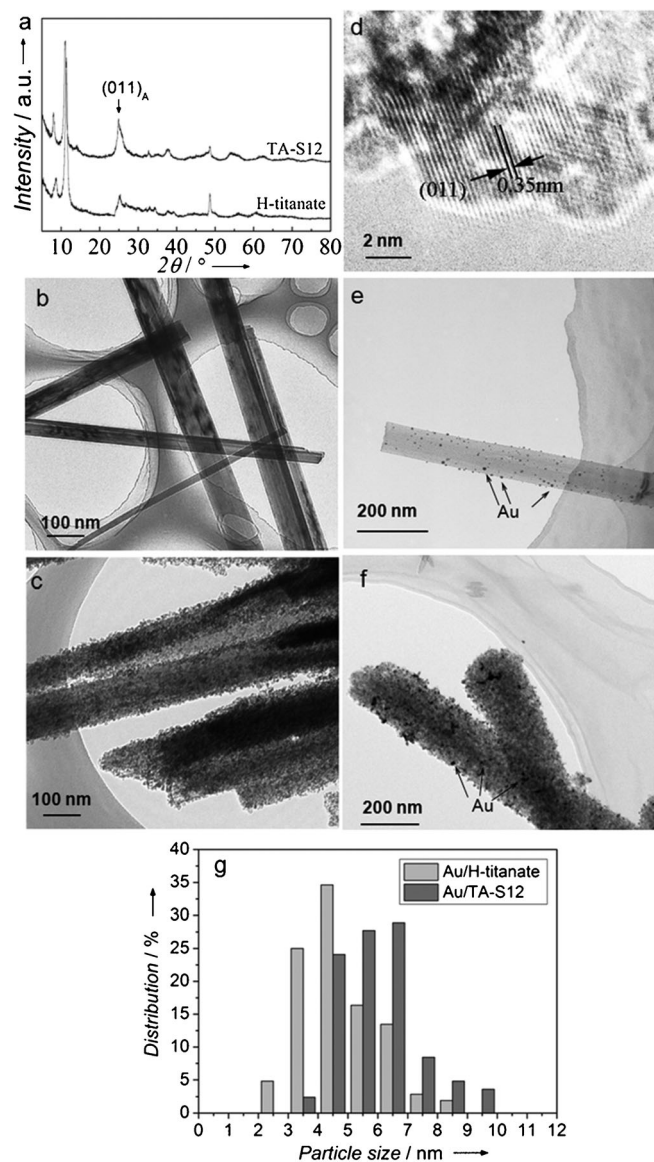


Figure 2. Structure and morphology of the samples. a) XRD patterns of H-titanate and TA-S12. b) TEM image of H-titanate NFs. c) TEM and d) HRTEM images of TA-S12. e) and f) TEM images of supported Au NPs on H-titanate and TA-S12, respectively. g) Particle size distributions of Au NPs on H-titanate and TA-S12.

tion peaks of a titanate acid^[33,34] rather than the peaks of anatase. The XRD pattern of this sample showed a broad hump, indicating an amorphous state. TEM images also indicated the change from amorphous particles (Figure S2a, 1 h product) to nanocrystals (Figure S2b, 12 h product) on H-titanate NFs. The amorphous solid formed first in the precursor and converted to anatase seeds that grew into nanocrystals during the hydrothermal process according to the XRD patterns in Figure 4a. An average crystallite size was estimated from XRD line broadening of anatase at 25.3° employing the Scherrer equation. The crystallite size at 1 h was 2.9 nm, increasing to 6.8 and 7.6 nm after the hydrothermal treatments of 12 h and 48 h, respectively. This calculated crystallite size matched well with the particle size observed in the TEM image (Figure 2c). For the

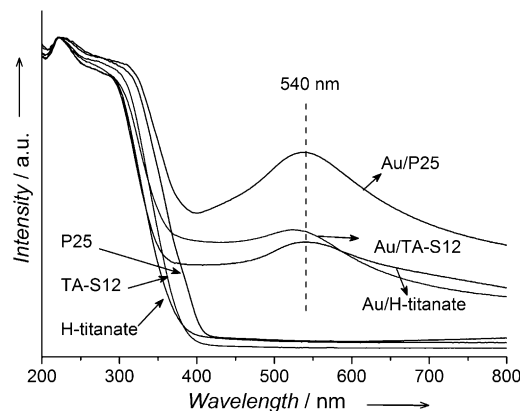


Figure 3. Normalized DRUV/Vis spectra of the supported Au NPs and the corresponding supports.

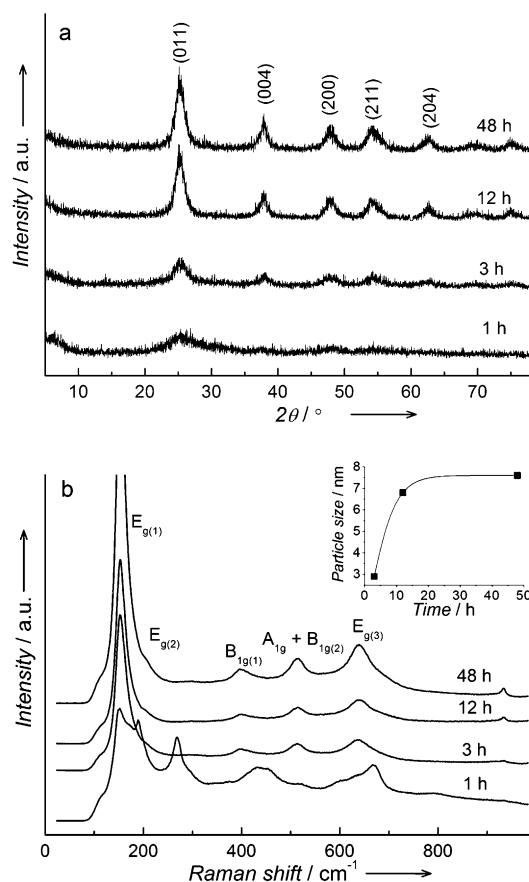


Figure 4. (a) XRD patterns and (b) Raman spectra of the solid samples precipitated from TiOSO_4 solution after treatment at 80°C for 1–48 h. The inset in Figure 4b illustrates the increase of the anatase particle size during the hydrothermal treatment.

sample, after 3 h hydrothermal reaction, six Raman active modes of anatase crystals were clearly seen: A_{1g} (515 cm^{-1}), $2B_{1g}$ (395 and 515 cm^{-1}) and $3E_g$ (152 , 199 , and 639 cm^{-1}).^[35] The blue shift of the strongest E_g mode from 144 cm^{-1} (for bulk anatase) to 152 cm^{-1} also indicated the formation of small anatase nanocrystals.^[36,37] The intensity increased slightly with the increasing hydrothermal treatment time. In a titanyl sulfate solution, TiO^{2+} [or $\text{Ti}(\text{OH})^{2+}$] is surrounded by H_2O .^[12,38,39] The

isoelectric point (IEP) of H-titanate was measured to be 5.4 at 25 °C, the detailed method is shown in the Supporting Information (Figure S3). At the acidic conditions used for the anatase NC painting (pH value below the IEP of H-titanate), the H-titanate NFs surfaces adsorb cations and become positively charged, analogous to other metal oxide surfaces.^[7,40,41] Therefore, at the beginning of the hydrothermal reaction, TiO_2^{2+} ions are adsorbed on the surface of the H-titanate NFs with hydration water (as proven by Raman spectra). In the subsequent step, the titanic acid loses the hydration water to form more stable anatase NCs.

We found that anatase NCs could also be grown on other oxide surfaces such as hollow spheres of fly ash (made largely of silica and alumina) and a layered clay, laponite (Figure 5).

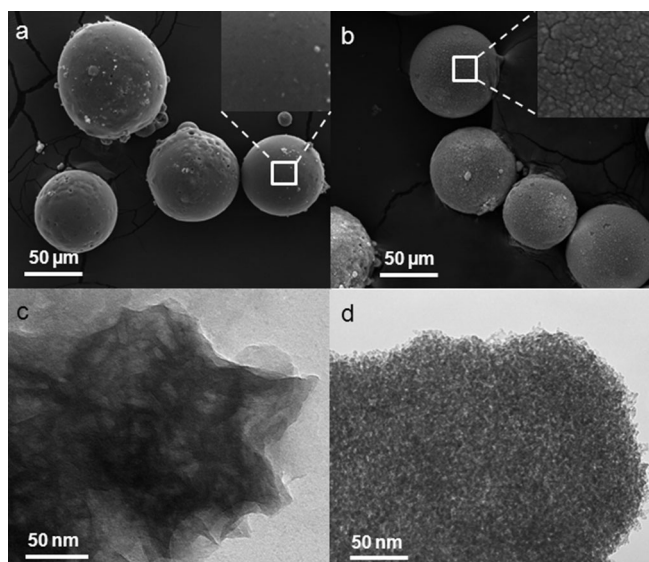


Figure 5. a, b) SEM images of fly-ash microballs and c, d) TEM images of laponite, before and after anatase nanoparticles painting, respectively. The insets in Figure 5a and 5b are enlarged SEM images.

Again, painting the anatase NC on laponite resulted in a significant increase of the specific surface area (from 345 to 463 $\text{m}^2 \text{g}^{-1}$). These results demonstrate that anatase NCs can be painted on a variety of oxide substrates. As most metal oxides have IEPs higher than 3,^[42] no further adjustment of the pH was required during the hydrothermal reaction for painting anatase NCs on the oxides by using titanyl sulfate solution.

In the TA-S12 sample, numerous anatase NCs were painted on H-titanate NFs. It is difficult to observe how the NCs attach onto the NFs by using HRTEM. Therefore, smaller amounts of anatase NCs were painted on H-titanate NFs by using a solution containing half as much of titanyl sulfate but maintaining

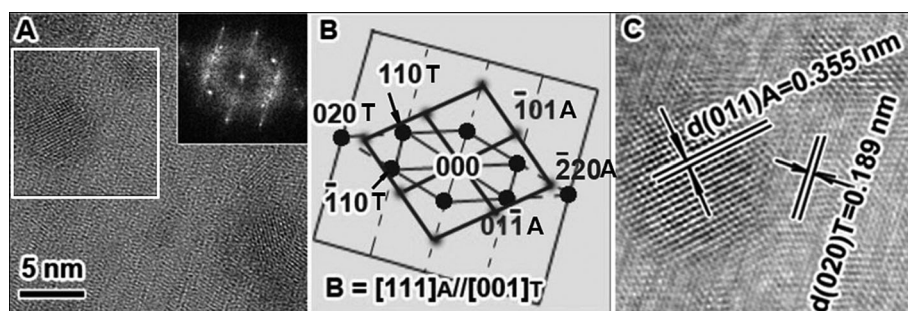


Figure 6. A) HRTEM image showing a single nanocrystal of anatase on the surface of H-titanate. The inset is an FFT image deduced from the red square area. B) Index of the FFT image in (A). The incident beam direction is $[111]_A/[001]_T$. C) The corresponding IFFT image derived from the red square area in (A). "A" and "T" represent anatase and H-titanate, respectively.

other reaction conditions identical to those for the preparation of TA-S12. According to HRTEM (Figure 6a) and fast Fourier transform analysis (FFT, Figure 6b), the anatase NCs were not randomly stacked on the surface of H-titanate NFs. The (110) planes in anatase NCs, $(110)_A$, were almost parallel with the (020) planes of the titanate fibers, $(020)_T$, with only a small angle divergence (less than 1°). This observation means that the anatase NC attached to the H-titanate fiber in such an orientation that (110) planes of the NCs are parallel to the (020) planes of the titanate, and thus the two phases can form a closely matched interface, so-called coherent interfaces.^[43–45] The oxygen atoms at the interface are shared by two phases. This interfacial match between anatase NCs and H-titanate NFs lowers the surface energy, which permits the anatase NCs to be bonded solidly onto the titanate fibers. The anatase NCs will not fall off from the H-titanate NFs if used during the catalytic reactions. This orientation of anatase NCs with respect to the H-titanate was different from what was previously observed.^[46,47]

Photocatalytic degradation of sulforhodamine B (SRB)

The photocatalytic activity of TA-S12 was compared with that of the well-known TiO_2 photocatalyst P25 (Degussa) for the degradation of the synthetic dye SRB under UV light (Figure 7). If equal amounts of the photocatalyst (0.5 g L^{-1}) were used, the

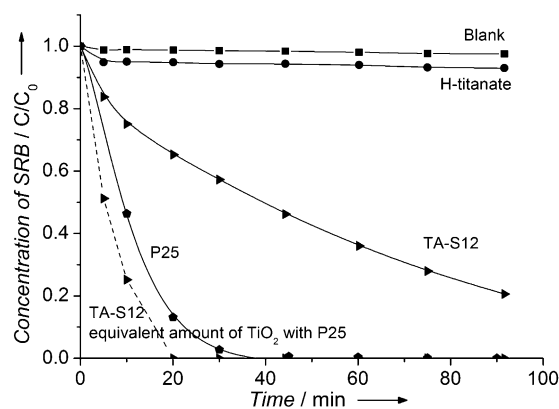


Figure 7. Photocatalytic degradation of SRB under UV light. The dashed line for TA-S12 was calculated by using the equivalent amount of TiO_2 in P25.

activity of TA-S12 was much lower than that of P25 under UV light irradiation. The H-titanate NFs exhibited negligible photoactivity for the degradation of SRB, and the TiO₂ content in TA-S12 was much lower than in P25 (which contains ≈80% anatase and ≈20% rutile). Anatase NCs accounted for approximately 26 wt% of the photocatalyst (calculated from the weight increase after NC painting). However, the photocatalytic activity of anatase NCs in TA-S12 was actually better than that of P25. If the mass of TA-S12 was 3.85 times of that of P25, the TiO₂ content in TA-S12 sample was equal to the TiO₂ content in P25. Under these circumstances, the activity of the TA-S12 sample was better than that of P25 (see Figure 7). There were two important factors influencing the activity: the amount of active sites and the rate of the photogenerated charge recombination.^[13,14] The number of the active sites depended mainly on the surface area of anatase and the more active sites the better the activity. The specific surface area for TA-S12 (166 m²g⁻¹) was much larger than for P25 (51 m²g⁻¹). This large specific surface area stemmed mainly from the anatase NCs because the H-titanate NFs had a specific surface area of 23 m²g⁻¹. The recombination rate was mainly affected by the crystal size. The smaller the crystal size, the faster the charge recombination (and thus the lower the activity).^[5,16,48] The size of the anatase NCs in TA-S12 (≈6 nm) was much smaller than in P25 (≈25 nm).^[49] The large surface area of TA-S12 is an advantage for the reactant adsorption providing more active sites for the reaction. However, the small sizes of anatase crystals in TA-S12 caused rapid recombination of the photogenerated electrons and holes. If the mean crystal size was 6.8 nm, the net result of the two offsetting factors was an improvement of the photocatalytic activity.

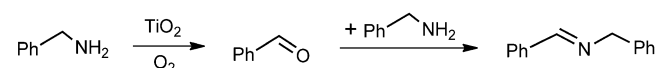
In addition, the sedimentation of TA-S12 NFs was compared with that of P25. As can be seen from Figure 8, the TA-S12 suspension became clear after 2 h sedimentation, whereas the P25 suspension was still turbid overnight. Thus, the TA-S12 NFs can be recovered for reuse readily but P25 cannot.

The anatase NC painted floating spheres of fly ash were also used for the degradation of SRB under UV light. The conversion rate after 4 h was 93.7%. The TiO₂ content on the painted fly ash was ≈25 wt% according to the energy dispersive X-ray measurement. The catalyst floated on the surface of the solution (Figure S4). This is an important advantage for practical

use because the photocatalyst can absorb light irradiation and contact with oxygen in air sufficiently and be readily separated after reaction.

Selective oxidation of benzylamine

TA-S12 also exhibited a high photocatalytic activity (conversion rate at 75% in 1 h) and product selectivity (to imine, >99%) for the selective oxidation of benzylamine in acetonitrile solvent under UV light illumination. This conversion rate was similar to that achieved with P25 (80%). Given that H-titanate was not active under the reaction conditions in the present study, the turnover frequency for the anatase NCs in TA-S12 (2.5 × 10⁻³ s⁻¹), calculated based on the total TiO₂ content, was much higher than that of P25 (6.9 × 10⁻⁴ s⁻¹). Actually, if 150 mg of TA-S12 (containing similar amounts of TiO₂ to a 50 mg sample of P25) was used for the reaction, TA-S12 showed a much better photocatalytic activity (85% conversion in 25 min) than P25 (80% conversion in 1 h). The reaction process involved two steps: a selective oxygenation to generate the aldehydes (the intermediate product, identified by GC-MS, Figure S5) and a subsequent aldehyde-amine condensation reaction to yield the imine.^[15,17]



The high selectivity was achieved because of the use of the inert solvent acetonitrile (to prevent the formation of OH[•] radicals and unselective autooxidation reactions). The large surface area of TA-S12 was an important factor contributing to the high conversion rate for the photocatalytic oxidation of benzylamine in the organic solvent.

Selective reduction of nitrobenzene on supported Au NPs

The photocatalytic performance of Au NPs on different supports for the reduction of nitrobenzene is summarized in Table 1. The photocatalyst exhibited activity only in the pres-

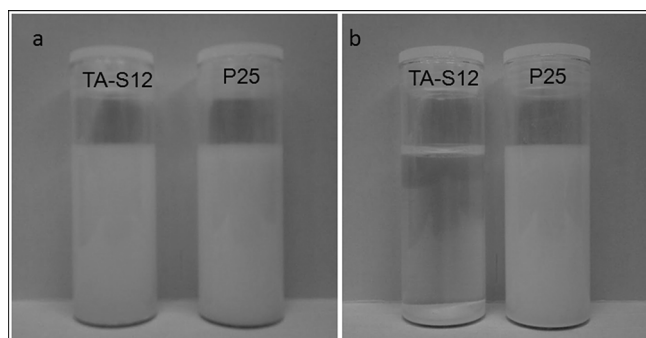


Figure 8. Photographs showing the sedimentation difference between TA-S12 and commercial P25: a) before and b) after 2 h sedimentation (concentration: 1 g L⁻¹ in water).

Table 1. Photocatalytic reduction of nitrobenzene using Au/TiO₂ under visible light.^[a]

	Product	Conversion [%]	Selectivity [%]	TOF ^[b] [s ⁻¹]
Au/TA-S12	azoxybenzene	50	> 99	5.5 × 10 ⁻³
Au/TA-S12 (no light)	azoxybenzene	25	> 99	2.7 × 10 ⁻³
Au/H-titanate	–	0	–	–
TA-S12	–	0	–	–
Au/P25	azoxybenzene	76	> 99	8.3 × 10 ⁻³
Au/P25 (no light)	azoxybenzene	55	> 99	6.0 × 10 ⁻³
P25	–	0	–	–

[a] Reaction conditions: catalyst (100 mg), nitrobenzene (1.5 mmol), isopropanol (15 mL) as the solvent, 0.1 M KOH/isopropanol (4.5 mL), reaction in argon gas under visible light (0.43 Wcm⁻²) at 40 °C for 5 h. [b] Turnover frequency.

ence of Au NPs. Both Au/TA-S12 and Au/P25 exhibited high conversions for the nitrobenzene reduction at 50% and 76%, respectively, in 5 h reaction time. The reaction on Au/TA-S12 and Au/P25 also proceeded in the dark, achieving conversions of 25% and 55%, respectively. An interesting finding was that azoxybenzene was the sole product if the photocatalyst of Au NPs on TiO₂ supports were used, whereas in our previous study, the azoxybenzene was the intermediate product and converted to azobenzene quickly on Au/ZrO₂.^[21] Evidently, the support materials significantly affect the product selectivity in the nitrobenzene reduction. Therefore, this finding can be utilized to prepare intermediate compounds, which are unstable to be obtained if catalysts at elevated temperatures are used. The photocatalyst of H-titanate supported Au NPs exhibited no activity for this reaction, also demonstrating the importance of the support materials on the performance of the photocatalyst. The phenomenon has not been fully understood yet, and further studies on the influence of the support materials is underway.

Conclusions

In summary, painting anatase nanocrystals (NCs) on a substrate is an efficient method that can be applied to various oxide substrates. It allowed us to achieve large photocatalytic active surfaces and solve the problems of particle aggregation and photocatalyst recovery. These two problems have seriously impeded the practical applications of the photocatalysts. The anatase NCs covered on H-titanate nanofibers (NFs) exhibited high activities for the degradation of sulforhodamine B, and high activities and selectivities (>99%) for the benzylamine oxidation (to imine). The photocatalysts of Au NPs on the anatase NC painted titanate NFs or on P25 could efficiently reduce nitrobenzene to azoxybenzene. Given that on Au NPs on ZrO₂ support under the same reaction conditions, the azoxybenzene is the intermediate product and quickly converts to azobenzene, the support material significantly affects the product selectivity of this reaction. Therefore, we can optimize the product selectivity by choice of the support materials. The photocatalysts with the nanofibril morphology are feasible for practical applications because they can be easily dispersed into a solution and separated from a liquid by filtration, sedimentation or centrifugation, because of their fibril morphology. The results of this study could be used for developing superior photocatalysts and other delicate functional nanostructures.

Experimental Section

Photocatalyst preparation

All the chemicals used in this study were analytical grade from Sigma-Aldrich unless otherwise stated and all the solutions were prepared by using high-purity deionized water (Millipore Corp., 18.2 MΩ cm). H-titanate was prepared by using the method published previously.^[50] TiOSO₄ solution was obtained by dissolving TiOSO₄·xH₂O (1.35 g, Fluka) in H₂O (10 mL). An aliquot of 0.5 mL of the above solution was diluted to 50 mL with H₂O and mixed with

H-titanate NFs (0.05 g). The mixture was kept at 80 °C for 12 h. After the reaction, the precipitate was collected and washed thoroughly with deionized water to remove residual SO₄²⁻ ions. Then the washed white solid was dried at 80 °C for 12 h. The sample was labeled as TA-S12. TiO₂ NCs were also painted on other materials such as laponite clay or fly ash by using the same approach. To prepare the Au NPs photocatalysts (3 wt%) on the fibril supports, H-titanate or TA-S12 (2.5 g) was dispersed into 3.8 × 10⁻³ M HAuCl₄ solution (100 mL), followed by addition of 0.53 M lysine (20 mL) under magnetic stirring. The stirring was prolonged for 30 min. To this suspension, 0.35 M NaBH₄ solution (10 mL) was added gradually, followed by addition of 0.3 M hydrochloric acid (10 mL). Then the mixture was aged for 12 h. Finally, the solid was separated, washed with deionized water and ethanol, and dried at 80 °C (labeled as Au/TA-S12).

Characterization

TEM was used to study the detailed structure of anatase NC painted H-titanate NFs. TEM and high-resolution TEM (HRTEM) were conducted on a Techni F20 transmission electron microscope operating at 200 kV. XRD patterns of the sample powders were recorded on a Philips PANalytical X'Pert PRO diffractometer using Cu_{Kα} radiation (λ = 1.5418 Å) operating at 40 kV and 40 mA with a fixed slit. Diffuse reflectance UV/Vis (DRUV/Vis) spectra of the samples were measured on a Varian Cary 5000 spectrometer. The Raman spectra of the samples were measured on a Spectra-Physics model 127 He-Ne laser (633 nm) at a resolution of 2 cm⁻¹. Nitrogen sorption isotherms were measured by the volumetric method on an automatic adsorption instrument (Micromeritics, Tristar 3000) at liquid nitrogen temperature (77 K). Zeta potential measurements were conducted on a Malvern nano-ZS zetasizer connected with a MPT-2 multipurpose titrator.

Photocatalytic degradation of sulforhodamine B

Six parallel Hg lamps (20W, NEC, FL20SBL) were used as the UV light source, and the peak of the wavelength was at approximately 350 nm. The catalyst concentration was 0.5 g L⁻¹, and the initial concentration (C₀) of the SRB was 1.8 × 10⁻⁵ M. At designed irradiation time intervals, specimens were taken from the reaction dispersion, and filtered through a Millipore filter (400 nm, Teflon) to remove the catalyst particles prior to the analysis. The filtrate was analyzed by UV/Vis spectra (Varian Cary 100 spectrometer) for the absorbance intensity by using the reading at 565 nm.

Photocatalytic oxidation of benzylamine

The UV source was a 100 W Hg lamp. Reactions were conducted in an oxygen atmosphere at 40 °C. In a typical reaction, benzylamine (0.2 mmol) was dissolved in acetonitrile (5 mL), to which the photocatalyst (50 mg) was added. The liquid products were analyzed by using an Agilent HP-6890 GC and GC-MS with an HP-5 column.

Photocatalytic reduction of nitrobenzene

The reduction of nitrobenzene was conducted in an argon atmosphere at 40 °C. In a typical reaction, nitrobenzene (1.5 mmol) was

dissolved in isopropyl alcohol (15 mL), and a solution of KOH in isopropyl alcohol (0.1 M, 4.5 mL) and the catalyst (50 mg) were added. Then, the reaction mixture was illuminated with incandescent light (mainly visible light, 0.43 W cm^{-2}) for 5 h under magnetic stirring. The liquid products were analyzed by using an Agilent HP-6890 GC with a HP-5 column.

Acknowledgements

Financial Supports from the Australian Research Council (ARC) is gratefully acknowledged. Prof Yingxin Xi and Dr Qin Zhou are highly acknowledged for providing of the fly ash and laponite samples. The authors acknowledge the facilities, and the scientific and technical assistance, of the Australian Microscopy & Microanalysis Research Facility at the Centre for Microscopy and Microanalysis, The University of Queensland.

Keywords: gold · nanostructures · photochemistry · supported catalysts · titanates

- [1] A. L. Linsebigler, G. Q. Lu, J. T. Yates, *Chem. Rev.* **1995**, *95*, 735–758.
- [2] M. R. Hoffmann, S. T. Martin, W. Y. Choi, D. W. Bahnemann, *Chem. Rev.* **1995**, *95*, 69–96.
- [3] M. A. Fox, M. T. Dulay, *Chem. Rev.* **1993**, *93*, 341–357.
- [4] K. Masao, O. Ichihiro, *Photocatalysis: Science and Technology*, Springer, New York, **2003**.
- [5] Z. Zhang, C.-C. Wang, R. Zakaria, J. Y. Ying, *J. Phys. Chem. B* **1998**, *102*, 10871–10878.
- [6] Z. F. Zheng, J. Teo, X. Chen, H. W. Liu, Y. Yuan, E. R. Waclawik, Z. Y. Zhong, H. Y. Zhu, *Chem. Eur. J.* **2010**, *16*, 1202–1211.
- [7] K. Takanabe, K. Domen, *ChemCatChem* **2012**, *4*, 1485–1497.
- [8] R. Kydd, W. Y. Teoh, J. Scott, D. Ferri, R. Amal, *ChemCatChem* **2009**, *1*, 286–294.
- [9] D. Beydoun, R. Amal, G. K. C. Low, S. McEvoy, *J. Phys. Chem. B* **2000**, *104*, 4387–4396.
- [10] H. Y. Zhu, X. P. Gao, Y. Lan, D. Y. Song, Y. X. Xi, J. C. Zhao, *J. Am. Chem. Soc.* **2004**, *126*, 8380–8381.
- [11] S. Yamabi, H. Imai, *Thin Solid Films* **2003**, *434*, 86–93.
- [12] S. Yamabi, H. Imai, *Chem. Mater.* **2002**, *14*, 609–614.
- [13] E. V. Skorb, D. G. Shchukin, H. Moehwald, D. V. Sviridov, *J. Mater. Chem.* **2009**, *19*, 4931–4937.
- [14] J. A. Byrne, B. R. Eggins, N. M. D. Brown, B. McKinney, M. Rouse, *Appl. Catal. B* **1998**, *17*, 25–36.
- [15] X. Lang, H. Ji, C. Chen, W. Ma, J. Zhao, *Angew. Chem.* **2011**, *123*, 4020–4023; *Angew. Chem. Int. Ed.* **2011**, *50*, 3934–3937.
- [16] M. Anpo, P. V. Kamat, *Environmentally Benign Photocatalysts: Applications of Titanium Oxide-based Materials*, Springer, London, **2010**.
- [17] X. Lang, W. Ma, Y. Zhao, C. Chen, H. Ji, J. Zhao, *Chem. Eur. J.* **2012**, *18*, 2624–2631.
- [18] V. Augugliaro, T. Caronna, V. Loddo, G. Marci, G. Palmisano, L. Palmisano, S. Yurdakal, *Chem. Eur. J.* **2008**, *14*, 4640–4646.
- [19] S. Yurdakal, G. Palmisano, V. Loddo, V. Augugliaro, L. Palmisano, *J. Am. Chem. Soc.* **2008**, *130*, 1568–1569.
- [20] X. Chen, H. Y. Zhu, J. C. Zhao, Z. F. Zheng, X. P. Gao, *Angew. Chem.* **2008**, *120*, 5433–5436; *Angew. Chem. Int. Ed.* **2008**, *47*, 5353–5356.
- [21] H. Y. Zhu, X. B. Ke, X. Z. Yang, S. Sarina, H. W. Liu, *Angew. Chem.* **2010**, *122*, 9851–9855; *Angew. Chem. Int. Ed.* **2010**, *49*, 9657–9661.
- [22] D. Tsukamoto, Y. Shiraishi, Y. Sugano, S. Ichikawa, S. Tanaka, T. Hirai, *J. Am. Chem. Soc.* **2012**, *134*, 6309–6315.
- [23] A. Gorrane, A. Corma, H. García, *Science* **2008**, *322*, 1661–1664.
- [24] A. Corma, P. Concepción, P. Serna, *Angew. Chem.* **2007**, *119*, 7404–7407; *Angew. Chem. Int. Ed.* **2007**, *46*, 7266–7269.
- [25] S. Patai, *The Chemistry of the Hydrato, Azo and Azoxy Groups*, Vol. 2, Wiley, Chichester, **1997**.
- [26] S.-I. Murahashi, *Angew. Chem.* **1995**, *107*, 2670–2693; *Angew. Chem. Int. Ed. Engl.* **1995**, *34*, 2443–2465.
- [27] K. S. W. Sing, D. H. Everett, R. A. W. Haul, L. Moscou, R. A. Pierotti, J. Rouquerol, T. Siemieniowska, *Pure Appl. Chem.* **1985**, *57*, 603–619.
- [28] Y. V. Kolen'ko, K. A. Kovnir, A. I. Gavrilo, A. V. Garshev, J. Frantti, O. I. Lebedev, B. R. Churagulov, G. VanTendeloo, M. Yoshimura, *J. Phys. Chem. B* **2006**, *110*, 4030–4038.
- [29] D. Wu, J. Liu, X. N. Zhao, A. D. Li, Y. F. Chen, N. B. Ming, *Chem. Mater.* **2006**, *18*, 547–553.
- [30] M. Quinten, *Optical Properties of Nanoparticle Systems: Mie and beyond*, Wiley-VCH, Weinheim, **2011**.
- [31] P. Mulvaney, *Langmuir* **1996**, *12*, 788–800.
- [32] A. S. K. Hashmi, G. J. Hutchings, *Angew. Chem.* **2006**, *118*, 8064–8105; *Angew. Chem. Int. Ed.* **2006**, *45*, 7896–7936.
- [33] T. Gao, H. Fjellvag, P. Norby, *Inorg. Chem.* **2009**, *48*, 1423–1432.
- [34] T. Beuvier, M. Richard-Plouet, L. Brohan, *J. Phys. Chem. C* **2010**, *114*, 7660–7665.
- [35] T. Ohsaka, F. Izumi, Y. Fujiki, *J. Raman Spectrosc.* **1978**, *7*, 321–324.
- [36] W. F. Zhang, Y. L. He, M. S. Zhang, Z. Yin, Q. Chen, *J. Phys. D* **2000**, *33*, 912–916.
- [37] M. A. Cortés-Jácome, G. Ferrat-Torres, L. F. F. Ortiz, C. Angeles-Chavez, E. Lopez-Salinas, J. Escobar, M. L. Mosqueira, J. A. Toledo-Antonio, *Catal. Today* **2007**, *126*, 248–255.
- [38] D. V. Bavykin, E. N. Savinov, P. G. Smirniotis, *React. Kinet. Catal. Lett.* **2003**, *79*, 77–84.
- [39] Y. Ohya, *Aqueous Precursors in Handbook of Sol-gel Science and Technology: Processing, Characterization and Application*, Vol. 1 (Ed.: H. Kozuka), Kluwer, Boston, **2005**, p. 108.
- [40] J.-P. Jolivet, *Metal Oxide Chemistry and Synthesis: From Solution to Solid State*, Wiley, New York, **2000**.
- [41] Case Studies of Nobel-Metal Catalysts. S. Soled in *Synthesis of Solid Catalysts*, (Ed.: K. P. de Jong), Wiley-VCH, Weinheim, **2009**, p. 355.
- [42] M. Kosmulski, *Chemical Properties of Material Surfaces*, CRC Press, New York, **2001**.
- [43] Y. Min, M. Akbulut, K. Kristiansen, Y. Golan, J. Israelachvili, *Nat. Mater.* **2008**, *7*, 527–538.
- [44] G. Renaud, *Surf. Sci. Rep.* **1998**, *32*, 5–90.
- [45] C. B. Eom, R. B. Vandover, J. M. Phillips, D. J. Werder, J. H. Marshall, C. H. Chen, R. J. Cava, R. M. Fleming, D. K. Fork, *Appl. Phys. Lett.* **1993**, *63*, 2570–2572.
- [46] H. W. Liu, Z. F. Zheng, D. J. Yang, X. B. Ke, E. Jaatinen, J. C. Zhao, H. Y. Zhu, *ACS Nano* **2010**, *4*, 6219–6227.
- [47] D. J. Yang, H. W. Liu, Z. F. Zheng, Y. Yuan, J. C. Zhao, E. R. Waclawik, X. B. Ke, H. Y. Zhu, *J. Am. Chem. Soc.* **2009**, *131*, 17885–17893.
- [48] M. Anpo, T. Shima, S. Kodama, Y. Kubokawa, *J. Phys. Chem.* **1987**, *91*, 4305–4310.
- [49] T. Ohno, K. Sarukawa, K. Tokieda, M. Matsumura, *J. Catal.* **2001**, *203*, 82–86.
- [50] Z. F. Zheng, H. W. Liu, J. P. Ye, J. C. Zhao, E. R. Waclawik, H. Y. Zhu, *J. Mol. Catal. A: Chem.* **2010**, *316*, 75–82.

Received: December 14, 2012


Revised: January 17, 2013

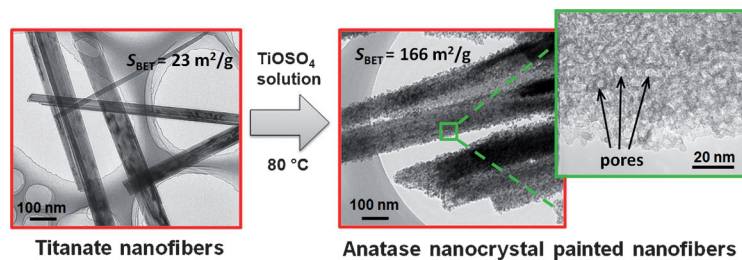
Published online on ■■■■■, 0000

FULL PAPERS

Z. Zheng, J. Zhao, H. Liu, J. Liu, A. Bo, H. Zhu*

■ ■ - ■ ■

 **Painting Anatase (TiO₂) Nanocrystals on Long Nanofibers to Prepare Photocatalysts with Large Active Surface for Dye Degradation and Organic Synthesis**



A porous paint: Anatase nanocrystals with large surface areas that were painted on the surface of titanate nanofibers bonded solidly. This process generated

a superior active surface for photocatalytic reactions, either serving as the photocatalyst or Au catalyst support.